JOURNAL OF SPACECRAFT AND ROCKETS
Vol. 37, No. 6, November–December 2000

Nonlinear Yaw–Pitch–Roll Coupling of Unguided Missiles with Wraparound Fins

Ömer Tanrıkulu,* Cenk Önen,† and Taner Gökhan‡
TÜBİTAK-SAGE, Defense Industries Research and Development Institute, 06261 Ankara, Turkey

Almost all of the research on flight dynamics of unguided missiles with wraparound fins is based on linear system models. This is in sharp contrast with the research on flight dynamics of planar finned unguided missiles, which has focused mostly on nonlinear problems since the 1950s. A general fifth-order nonlinear autonomous dynamic system model is developed for unguided missiles with four wraparound fins. Aerodynamic characteristics of a basic planar finner and a basic wraparound finner are obtained by using a panel code, Missile DATCOM empirical database, and published experimental data. Effects of nonlinear aerodynamic terms on location and stability of equilibrium points of a basic planar finner and a basic wraparound finner are investigated. It is shown that wraparound and planar finned unguided missiles have different aerodynamic and flight dynamic characteristics.

Nomenclature

a_D	=	quadratic drag force coefficient
a_F, b_F	=	cubic transverse static force coefficients
a_t, b_t	=	cubic transverse static moment coefficients
a_∞	=	freestream speed of sound, m/s
C_D	=	drag force coefficient
C_{D_0}	=	drag force coefficient for $\delta = 0$
C_F	=	$C_Y + iC_Z$
C_l, C_m, C_n	=	aerodynamic moment coefficients
C_{l_p}	=	roll damping moment stability derivative, $[\partial C_l / \partial (p\lambda/2v_C)]$
C_{l_0}	=	induced roll moment coefficient
$C_{l_{\delta f}}$	=	roll moment stability derivative with respect to fin cant
C_{M_0}	=	$\sqrt{(C_{m_0}^2 + C_{n_0}^2)}$
C_{m_q}, C_{m_r}	=	transverse damping moment stability derivatives
C_{m_0}, C_{n_0}	=	asymmetry moment coefficients
C_{m_α}, C_{m_β}	=	transverse static moment stability derivatives
$C_{m_{\alpha p}}$, $C_{m_{\beta p}}$	=	Magnus moment stability derivatives
$C_{m_{\dot\alpha}}$, $C_{m_{\dot\beta}}$	=	transverse lag moment stability derivatives
$C_{m_{\delta^2\gamma}}$	=	transverse induced moment coefficient
C_t	=	$C_m + iC_n$
C_X, C_Y, C_Z	=	aerodynamic force coefficients
C_{Y_0}, C_{Z_0}	=	asymmetry force coefficients
C_{Z_q}, C_{Z_r}	=	transverse damping force stability derivatives
C_{Z_α}, C_{Z_β}	=	static force stability derivatives
$C_{Z_{\alpha p}}$, $C_{Z_{\beta p}}$	=	Magnus force stability derivatives
$C_{Z_{\dot\alpha}}$, $C_{Z_{\dot\beta}}$	=	transverse lag force stability derivatives
$C_{Z_{\delta^2\gamma}}$	=	transverse induced force coefficient
c	=	$\sqrt{[-M_0/(1-\sigma)]}$
c_F, d_F	=	cubic transverse damping force coefficients
c_t, d_t	=	cubic transverse damping moment coefficients
D_m	=	missile diameter, m
e_F, f_F	=	cubic Magnus force coefficients
e_t, f_t	=	cubic Magnus moment coefficients
F_b	=	body-fixed reference frame
$g_2 + ig_3$	=	transverse components of gravitational acceleration vector, m/s^2
I_a, I_t	=	axial and transverse moments of inertia, kg m^2
k_a, k_t	=	nondimensional axial and transverse radii of gyration
M_∞	=	freestream Mach number
m	=	mass, kg
p, q, r	=	rotational velocity components, rad/s
r_C	=	nondimensional transverse distance of center of mass from geometrical center of missile cross section
S_m	=	reference area, $(\pi/4)\lambda^2$, m^2
s	=	nondimensional distance variable, $s = \frac{1}{\lambda}\int_{t_0}^{t} v_C \, dt$
t	=	time, s
u, v, w	=	translational velocity components, m/s
$\boldsymbol{u}_{1,2,3}^{(b)}$	=	unit vectors of F_b
v_C	=	speed of missile, $\sqrt{(u^2 + v^2 + w^2)}$, m/s
x_{cm}	=	center of mass location from missile nose tip, m
α	=	w/v_C
β	=	v/v_C
δ_f	=	fin cant angle
ζ	=	$\xi/\delta_{T_R} = \delta_s e^{i\gamma}$
λ	=	reference length, missile diameter, D_m, m
μ	=	$(q\lambda/2v_C) + i(r\lambda/2v_C) = \varepsilon e^{i\eta}$
ξ	=	$\beta + i\alpha = \delta e^{i\gamma}$
ρ_∞	=	freestream density, kg/m^3
σ	=	I_a/I_t
τ	=	nondimensional distance variable; Eq. (48)
ϕ_M	=	$\tan^{-1}(C_{n_0}/C_{m_0})$
ψ, θ, ϕ	=	Euler yaw, pitch, roll angles

Superscripts

(I)	=	imaginary component
(R)	=	real component
T	=	matrix transpose
$*$	=	multiplication with $\rho_\infty S_m \lambda/2m$
$\frown$	=	division by c
$-$	=	complex conjugate
$\cdot$	=	differentiation with respect to t or τ

Received 1 May 1999; revision received 20 July 2000; accepted for publication 27 July 2000.

*Coordinator, Mechanics and Systems Engineering Research Group, PK 16, Mamak. Member AIAA.

†Chief Research Engineer, External Ballistics Section, Mechanics and Systems Engineering Research Group, PK 16, Mamak; currently Aeronautical Engineer, Engineering Development Group, ROKETSAN AŞ, Missile Industries, Inc., P.O. Box 30, Elmadağ, Ankara, Turkey.

‡Chief Research Engineer, External Ballistics Section, Mechanics and Systems Engineering Research Group, PK 16, Mamak.

Introduction

FLIGHT dynamics of unguided missiles with wraparound fins (WAF) is much more complicated when compared to that of planar finned (PF) configurations. This is due to the lack of mirror symmetry of unguided missiles with WAF. Flight dynamicists have mostly used linear system models to examine WAF configurations.[1–11] Very few researchers focused on nonlinear

problems related to WAF.[12,13] This is surprising considering the intensity of post-World War II research on nonlinear flight dynamics of unguided missiles with PF, which have both rotational and mirror symmetry. Lack of attention to nonlinear flight dynamics of WAF configurations may be attributed to difficulties that have been experienced even in determination of aerodynamic data for linear models. Widely used engineering codes for prediction of missile aerodynamics such as Missile DATCOM do not have the capability for WAF even though WAF has become a standard design feature of tube-launched unguided missiles all over the world (2.75-in. Hydra-70, 5-in. Zuni, 9-in. MLRS, 160-mm RAYO, 300-mm Smerch, etc.).

One of the most important problems in nonlinear flight dynamics of unguided missiles with PF has been coupling between yaw, pitch, and roll degrees of freedom due to nonlinear aerodynamic properties and configurational asymmetries. Such coupling can cause sustained transverse resonant oscillations with large amplitude (lock-in), which sometimes end with a severe dynamic instability (catastrophic yaw).[14–35] The aim of this study is development of a nonlinear flight dynamics model for configurations with four WAF that can be used to analyze lock-in and catastrophic yaw problems. A general nonlinear aerodynamics model for unguided missiles with WAF is obtained by using the well-known Maple–Synge analysis (see Ref. 36). In derivation of flight dynamics equations of motion, previous research[33–35] on yaw–pitch–roll coupling of unguided missiles with PF is followed. Attention is focused on equilibrium behavior, and location of equilibrium points is determined graphically for simple cases and iteratively for more complicated ones. Stability of equilibrium points is determined by using linearization. Aerodynamic and flight dynamic characteristics of a basic planar finner and a basic wraparound finner are examined for flight at a Mach number of $M_\infty = 3.0$.

Maple–Synge Analysis

One of the main problems in analyzing dynamics of a flying vehicle is mathematical modeling of the relationship between aerodynamic forces and moments that act on the vehicle and on translational and rotational velocities of the vehicle. Aerodynamic modeling is relatively simple in the case of unguided missiles that almost always have a large level of geometrical symmetry with respect to their longitudinal axes. In Fig. 1, cross-sectional views of two unguided missiles are shown. The missile with four PF (configuration A) has four-gonal rotational symmetry and four planes of mirror symmetry, and it is known as the cruciform configuration. The missile with four WAF (configuration B) also has four-gonal rotational symmetry, but it lacks mirror symmetry. Maple–Synge analysis is an elegant mathematical tool that simplifies aerodynamic modeling of unguided missiles by using rotational and mirror symmetry properties.[36] Nondimensional transverse and axial force and moment coefficients are assumed to have the following form in Maple–Synge analysis:

$$C_{(F,t,X,l)} = \sum_{ijkl} (f, t, x, l)_{ijkl} \xi^i \bar{\xi}^j \mu^k \bar{\mu}^l \tag{1}$$

where f_{ijkl}, t_{ijkl}, x_{ijkl}, and l_{ijkl} are complex functions of u/v_C and $p\lambda/2v_C$. In C_F, C_t, C_X and C_l expansions, there is potentially 1 term for $D = 0$, 4 terms for $D = 1$, 10 terms for $D = 2$, and 20 terms for $D = 3$, where $D = i + j + k + l$. Maple–Synge analysis shows that only 12 and 5 out of 35 of these terms are admissible for (C_F, C_t) and (C_X, C_l), respectively, for a configuration with four-gonal rotational symmetry. Admissible C_F expansion including and up to terms with $D = 3$ is as follows for both configurations A and B:

$$\begin{aligned} C_F = {} & f_{1000}\xi + f_{0010}\mu + f_{0003}\bar{\mu}^3 + f_{0102}\bar{\xi}\bar{\mu}^2 + f_{0201}\bar{\xi}^2\bar{\mu} \\ & + f_{0300}\bar{\xi}^3 + f_{2001}\xi^2\bar{\mu} + f_{2100}\xi^2\bar{\xi} + f_{1011}\xi\mu\bar{\mu} \\ & + f_{1110}\xi\bar{\xi}\mu + f_{0021}\mu^2\bar{\mu} + f_{0120}\bar{\xi}\mu^2 \end{aligned} \tag{2}$$

Admissible C_t expansion has the same structure as the earlier C_F expansion. Admissible C_X expansion including and up to terms with $D = 3$ is as follows for both configurations A and B:

$$C_X = x_{0000} + x_{0011}\mu\bar{\mu} + x_{1001}\xi\bar{\mu} + x_{0110}\bar{\xi}\mu + x_{1100}\xi\bar{\xi} \tag{3}$$

Admissible C_l expansion has the same structure as the earlier C_X expansion. Note that there are no even admissible terms ($D = 0, 2, 4, \ldots$) for C_F and C_t, whereas there are no odd admissible terms ($D = 1, 3, 5, \ldots$) for C_X and C_l in case of four-gonal rotational symmetry.

In conventional flight dynamics analysis, the terms of C_F and C_t expansions with the following indices have been neglected even though they are admissible: 0003, 0102, 0201, 2001, 1011, 0021, and 0120. Moreover, dependence of the remaining f_{ijkl} and t_{ijkl} on $p\lambda/2v_C$ is neglected except in the case of f_{1000} and t_{1000}, which are mostly assumed to be linear functions of $p\lambda/2v_C$. Hence, C_F and C_t expansions can be written as

$$\begin{aligned} C_F = {} & C_{Z_\alpha}\left(1 + a_F\delta^2\right)\xi + iC_{Z_\beta}\left(1 + b_F\delta^2\right)\xi + C_{Z_r}\left(1 + c_F\delta^2\right)\mu \\ & + iC_{Z_q}\left(1 + d_F\delta^2\right)\mu + C_{Z_{\alpha p}}\left(1 + e_F\delta^2\right)(p\lambda/2v_C)\xi \\ & + iC_{Z_{\beta p}}\left(1 + f_F\delta^2\right)(p\lambda/2v_C)\xi + \left(C^{(R)}_{Z_{\delta^2\gamma}} + iC^{(I)}_{Z_{\delta^2\gamma}}\right)\delta^2 e^{-i4\gamma}\xi \end{aligned} \tag{4}$$

$$\begin{aligned} C_t = {} & -iC_{m_\alpha}\left(1 + a_t\delta^2\right)\xi + C_{m_\beta}\left(1 + b_t\delta^2\right)\xi - iC_{m_r}\left(1 + c_t\delta^2\right)\mu \\ & + C_{m_q}\left(1 + d_t\delta^2\right)\mu - iC_{m_{\alpha p}}\left(1 + e_t\delta^2\right)(p\lambda/2v_C)\xi \\ & + C_{m_{\beta p}}\left(1 + f_t\delta^2\right)(p\lambda/2v_C)\xi + \left(C^{(R)}_{m_{\delta^2\gamma}} + iC^{(I)}_{m_{\delta^2\gamma}}\right)\delta^2 e^{-i4\gamma}\xi \end{aligned} \tag{5}$$

Equation (4) will be simplified by neglecting the terms that are characterized by C_{Z_β}, C_{Z_r}, C_{Z_q}, $C_{Z_{\alpha p}}$, and $C_{Z_{\beta p}}$ because previous experience shows that they drop out from the analysis during derivation of aeroballistic equations of motion through multiplication with the density factor $\rho_\infty S_m \lambda/2m$ (Ref. 37). The literature on aerodynamics and flight dynamics of unguided missiles with WAF show that the moment associated with C_{m_β} is much smaller than the one associated with C_{m_α}. The same relationship can be assumed to exist between the moments characterized by (C_{m_r}, $C_{m_{\alpha p}}$) and (C_{m_q}, $C_{m_{\beta p}}$), respectively. Because the moments characterized by (C_{m_q}, $C_{m_{\beta p}}$) are already small, the ones associated with (C_{m_r}, $C_{m_{\alpha p}}$) will be neglected. The aerodynamic memory effect will be taken into account by adding the $-iC_{m_{\dot\alpha}}(\dot\xi\lambda/2v_C)$ term into the C_t expansion. $C_{Z_{\dot\beta}}$, $C_{Z_{\dot\alpha}}$, and $C_{m_{\dot\beta}}$ will be neglected based on arguments that are similar to the ones presented earlier. Note that superscript overdot denotes differentiation with respect to t in $C_{Z_{\dot\beta}}$, $C_{Z_{\dot\alpha}}$, $C_{m_{\dot\beta}}$, and $C_{m_{\dot\alpha}}$. Slight configurational asymmetries will be modeled by adding bias terms $C_{Y_0} + iC_{Z_0}$ and $C_{m_0} + iC_{n_0}$ to C_F and C_t expansions, respectively. Hence, the final form of the transverse aerodynamics model for an unguided missile with four-gonal rotational symmetry only (configuration B) becomes

$$\begin{aligned} C_F = {} & \left(C_{Y_0} + iC_{Z_0}\right) + C_{Z_\alpha}\left(1 + a_F\delta^2\right)\xi \\ & + \left(C^{(R)}_{Z_{\delta^2\gamma}} + iC^{(I)}_{Z_{\delta^2\gamma}}\right)\delta^2 e^{-i4\gamma}\xi \end{aligned} \tag{6}$$

$$\begin{aligned} C_t = {} & \left(C_{m_0} + iC_{n_0}\right) - iC_{m_\alpha}\left(1 + a_t\delta^2\right)\xi + C_{m_\beta}\left(1 + b_t\delta^2\right)\xi \\ & + C_{m_q}\left(1 + d_t\delta^2\right)\mu + C_{m_{\beta p}}\left(1 + f_t\delta^2\right)(p\lambda/2v_C)\xi \\ & - iC_{m_{\dot\alpha}}(\dot\xi\lambda/2v_C) + \left(C^{(R)}_{m_{\delta^2\gamma}} + iC^{(I)}_{m_{\delta^2\gamma}}\right)\delta^2 e^{-i4\gamma}\xi \end{aligned} \tag{7}$$

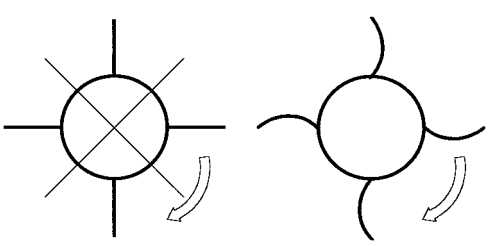

Configuration A Configuration B

Fig. 1 Rotational and mirror symmetry.

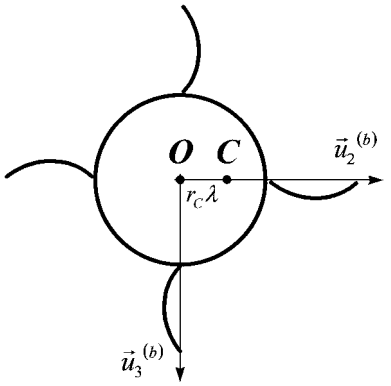

Fig. 2 Center of mass offset.

In Eqs. (6) and (7), all coefficients and stability derivatives are functions of u/v_C.

In conventional flight dynamics analysis, the terms of C_X expansion with the following indices have been neglected even though they are admissible: 0011, 1001, and 0110. Moreover, dependence of the remaining x_{ijkl} on $p\lambda/2v_C$ is neglected. Hence, C_D which is approximately equal to the negative of C_X for relatively small δ, can be written as

$$C_D = C_{D_0}\left(1 + a_D\delta^2\right) \tag{8}$$

In conventional flight dynamics analysis, all nonlinear terms of C_l expansion have been neglected:

$$C_l = C_{l_p}(p\lambda/2v_C) + C_{l_{\delta_f}}\delta_f \tag{9}$$

In Eq. (9) both C_{l_p} and $C_{l_{\delta_f}}$ will be assumed to be functions of u/v_C only. Roll aerodynamics will be modified by adding an asymmetry moment due to C_F acting through center of mass C, which is laterally offset from geometrical center O of the missile cross section as shown in Fig. 2. Previous studies show that missiles with WAF have a nonzero roll moment C_{l_0} even for $\delta = 0$. C_{l_0} is a complicated function of ξ and M_∞. Hence, the final form of the C_l expansion for an unguided missile with four-gonal rotational symmetry only (configuration B) can be derived as

$$C_l = C_{l_0} + C_{l_p}(p\lambda/2v_C) + C_{l_{\delta_f}}\delta_f + (r_C/2)\Big[iC_{Z_\alpha}\left(1 + a_F\delta^2\right) \times(\xi - \bar{\xi}) - iC^{(R)}_{Z_{\delta^2\gamma}}(\xi^3 - \bar{\xi}^3) - C^{(I)}_{Z_{\delta^2\gamma}}(\xi^3 + \bar{\xi}^3)\Big] \tag{10}$$

Previous studies show that roll damping moment of an unguided missile with WAF is roll direction dependent: $C_{l_{p+}}$ for $p > 0$ and $C_{l_{p-}}$ for $p < 0$. Magnus moment of a WAF configuration is also very likely to be roll direction dependent. It is relatively easy to determine $C_{l_{p+}}$ and $C_{l_{p-}}$ by using a panel code. On the other hand, accurate $C_{m_{\beta p+}}$ and $C_{m_{\beta p-}}$ data can only be determined experimentally. In this study roll direction dependence of both C_{l_p} and $C_{m_{\beta p}}$ will be neglected for simplicity.

Maple–Synge analysis can be used to determine the aerodynamic model of configuration A, which is much simpler compared to configuration B due to the additional mirror symmetry:

$$C_F = \left(C_{Y_0} + iC_{Z_0}\right) + C_{Z_\alpha}\left(1 + a_F\delta^2\right)\xi + C_{Z_{\delta^2\gamma}}\delta^2 e^{-i4\gamma}\xi \tag{11}$$

$$C_t = \left(C_{m_0} + iC_{n_0}\right) - iC_{m_\alpha}\left(1 + a_t\delta^2\right)\xi + C_{m_q}\left(1 + d_t\delta^2\right)\mu - iC_{m_\alpha}(\dot{\xi}\lambda/2v_C) + C_{m_{\beta p}}\left(1 + f_t\delta^2\right)(p\lambda/2v_C)\xi + iC_{m_{\delta^2\gamma}}\delta^2 e^{-i4\gamma}\xi \tag{12}$$

$$C_l = C_{l_p}(p\lambda/2v_C) + C_{l_{\delta_f}}\delta_f + i(r_C/2)C_{Z_\alpha}\left(1 + a_F\delta^2\right)(\xi - \bar{\xi}) - i(r_C/2)C_{Z_{\delta^2\gamma}}(\xi^3 - \bar{\xi}^3) \tag{13}$$

C_D expansion for configuration A will be the same as Eq. (8). Note that $C_{Z_{\delta^2\gamma}}$ and $C_{m_{\delta^2\gamma}}$ in Eqs. (11–13) are real coefficients.

Equations of Motion

Scaled transverse and axial rotational equations of motion, respectively, of a rigid, four-gonal unguided missile with WAF were derived as follows for a short-duration segment of approximately straight flight with constant v_C over a flat Earth:

$$\ddot{\zeta} + \left[\left(\hat{H}_0 + \hat{H}_{2_s}\delta_s^2\right) + i(2-\sigma)\dot{\phi}\right]\dot{\zeta} + \left\{i\ddot{\phi} + (1-\sigma)\left[1 - \dot{\phi}^2 + i\dot{\phi}\left(h_0 + h_{2_s}\delta_s^2\right)\right]\right\}\zeta - (1-\sigma)\left[m_{2_s}\delta_s^2 + i\left(n_0 + n_{2_s}\delta_s^2\right)\right]\zeta + i(s_i\dot{\phi} - r_i)\bar{\zeta}^3 = \Gamma\dot{\phi} + (1-\sigma)h_0\exp[i(\phi_M - \pi/2)] \tag{14}$$

$$\ddot{\phi} + \hat{K}_{p_0}\dot{\phi} + \kappa_{p_2}\delta_s^2\dot{\phi} = \hat{\bar{K}}_d + i\kappa_{\gamma_1}(\zeta - \bar{\zeta}) + i\kappa_{\gamma_2}\delta_s^2(\zeta - \bar{\zeta}) - i\kappa_{\gamma_3}(\zeta^3 - \bar{\zeta}^3) - \kappa_{\gamma_4}(\zeta^3 + \bar{\zeta}^3) \tag{15}$$

Coefficients of Eq. (14) can be obtained from the following:

$$H_0 = -2C^*_{D_0} - C^*_{Z_\alpha} - \frac{1}{2k_t^2}\left(C^*_{m_q} + C^*_{m_{\dot{\alpha}}}\right) \tag{16}$$

$$H_2 = -2C^*_{D_0}a_D - C^*_{Z_\alpha}a_F - \frac{1}{2k_t^2}C^*_{m_q}d_t \tag{17}$$

$$M_0 = \frac{1}{k_t^2}C^*_{m_\alpha} \tag{18}$$

$$M_2 = \frac{1}{k_t^2}C^*_{m_\alpha}a_t \tag{19}$$

$$N_0 = \frac{1}{k_t^2}C^*_{m_\beta} \tag{20}$$

$$N_2 = \frac{1}{k_t^2}C^*_{m_\beta}b_t \tag{21}$$

$$T_0 = \frac{1}{2k_a^2}C^*_{m_{\beta p}} - C^*_{Z_\alpha} - C^*_{D_0} \tag{22}$$

$$T_2 = \frac{1}{2k_a^2}C^*_{m_{\beta p}}f_t - C^*_{Z_\alpha}a_F - C^*_{D_0}a_D \tag{23}$$

$$S = \left(C^{(R)^*}_{Z_{\delta^2\gamma}} + iC^{(I)^*}_{Z_{\delta^2\gamma}}\right)\left[1 - 4\left(\frac{k_t}{k_a}\right)^2\right] \tag{24}$$

$$R = \frac{1}{k_t^2}\left(C^{(R)^*}_{m_{\delta^2\gamma}} + iC^{(I)^*}_{m_{\delta^2\gamma}}\right) \tag{25}$$

$$Q = 3\left(C^{(R)^*}_{Z_{\delta^2\gamma}} + iC^{(I)^*}_{Z_{\delta^2\gamma}}\right) \tag{26}$$

$$\hat{H}_{2_s} = \hat{H}_2\delta^2_{T_R} \tag{27}$$

$$h_0 = \frac{\hat{H}_0 - \sigma\hat{T}_0}{1-\sigma} \tag{28}$$

$$h_{2_s} = \frac{\hat{H}_2 - \sigma\hat{T}_2}{1-\sigma}\delta^2_{T_R} \tag{29}$$

$$m_{2_s} = \frac{\hat{\bar{M}}_2}{1-\sigma}\delta^2_{T_R} \tag{30}$$

$$n_0 = \frac{\hat{\bar{N}}_0}{1-\sigma} \tag{31}$$

$$n_{2_s} = \frac{\hat{\bar{N}}_2}{1-\sigma}\delta^2_{T_R} \tag{32}$$

$$s_i = (\sigma\hat{S} + \hat{Q})\delta^2_{T_R} \tag{33}$$

$$r_i = \hat{\bar{R}}\delta^2_{T_R} \tag{34}$$

$$\Gamma = -i\frac{\sigma\lambda}{c\delta_{T_R}v_C^2}(g_2 + ig_3) \tag{35}$$

Coefficients of Eq. (15) can be obtained from the following:

$$K_{p0} = -\left[C^*_{D_0} + \left(1/2k_a^2\right)C^*_{l_p}\right] \tag{36}$$

$$K_{p2} = -C^*_{D_0}a_D \tag{37}$$

$$K_d = \left(1/k_a^2\right)\left(C^*_{l_0} + C^*_{l_{\delta_f}}\delta_f\right) \tag{38}$$

$$K_{\gamma_1} = \left(r_C/2k_a^2\right)C^*_{Z_\alpha} \tag{39}$$

$$K_{\gamma_2} = \left(r_C/2k_a^2\right)C^*_{Z_\alpha}a_F \tag{40}$$

$$K_{\gamma_3} = \left(r_C/2k_a^2\right)C^{(R)^*}_{Z_{\delta^2\gamma}} \tag{41}$$

$$K_{\gamma_4} = \left(r_C/2k_a^2\right)C^{(I)^*}_{Z_{\delta^2\gamma}} \tag{42}$$

$$\kappa_{p2} = \bar{K}_{p2}\delta^2_{T_R} \tag{43}$$

$$\kappa_{\gamma_1} = \bar{\bar{K}}_{\gamma_1}\delta_{T_R} \tag{44}$$

$$\kappa_{\gamma_2} = \bar{\bar{K}}_{\gamma_2}\delta^3_{T_R} \tag{45}$$

$$\kappa_{\gamma_3} = \bar{\bar{K}}_{\gamma_3}\delta^3_{T_R} \tag{46}$$

$$\kappa_{\gamma_4} = \bar{\bar{K}}_{\gamma_4}\delta^3_{T_R} \tag{47}$$

In Eqs. (14) and (15), the overdot denotes differentiation with respect to nondimensional distance variable τ, which is defined as

$$\tau = cs = \left[\sqrt{-M_0/(1-\sigma)}\right]s \tag{48}$$

Here δ_{T_R} is amplitude of trim ξ at resonance when nonlinearity, gravity, and C_{m_β} are neglected:

$$\delta_{T_R} = \delta_{T_0}/h_0 \tag{49}$$

and δ_{T_0} is amplitude of trim ξ when nonlinearity, gravity, and C_{m_β} are neglected, and $p = 0$:

$$\delta_{T_0} = C_{M_0}/C_{m_\alpha} \tag{50}$$

Equilibrium Points

Equations of motion (14) and (15) can be expressed in state-space form as follows:

$$\dot{\boldsymbol{x}} = \boldsymbol{f}(\boldsymbol{x}), \qquad \boldsymbol{x} \in R^5, \qquad \boldsymbol{f}: R^5 \rightarrow R^5 \tag{51}$$

where

$$x_1 = \phi \tag{52}$$

$$x_2 + ix_3 = \zeta^{(R)} + i\zeta^{(I)} = \bar{\beta} + i\bar{\alpha} \tag{53}$$

$$x_4 + ix_5 = \dot{x}_2 + i\dot{x}_3 = \dot{\zeta}^{(R)} + i\dot{\zeta}^{(I)} = \dot{\bar{\beta}} + i\dot{\bar{\alpha}} \tag{54}$$

Equation (51) represents a fifth-order autonomous dynamic system. Equilibrium points of this system can be determined by solving

$$\boldsymbol{f}(\boldsymbol{x}_{\text{eq}}) = \boldsymbol{0} \tag{55}$$

by using the Newton–Raphson algorithm:

$$\boldsymbol{x}_{k+1} = \boldsymbol{x}_k - \boldsymbol{J}(\boldsymbol{x}_k)^{-1}\boldsymbol{f}(\boldsymbol{x}_k) \qquad (k = 0, 1, 2, \ldots) \tag{56}$$

The element of the Jacobian matrix $\boldsymbol{J}(\boldsymbol{x})$ at the ith row and the jth column can be obtained as follows:

$$J_{ij} = \frac{\partial f_i}{\partial x_j} \tag{57}$$

The stability of the system around a given equilibrium point $\boldsymbol{x}_{\text{eq}}$ can be determined by examining the time evolution of a small perturbation $\delta\boldsymbol{x}$:

$$\boldsymbol{x} = \boldsymbol{x}_{\text{eq}} + \delta\boldsymbol{x} \tag{58}$$

$$\dot{\boldsymbol{x}}_{\text{eq}} + \delta\dot{\boldsymbol{x}} \approx \boldsymbol{f}(\boldsymbol{x}_{\text{eq}}) + \boldsymbol{J}(\boldsymbol{x}_{\text{eq}})\delta\boldsymbol{x} \tag{59}$$

$$\delta\dot{\boldsymbol{x}} \approx \boldsymbol{J}(\boldsymbol{x}_{\text{eq}})\delta\boldsymbol{x} \tag{60}$$

Hence, eigenvalues of $\boldsymbol{J}(\boldsymbol{x}_{\text{eq}})$ indicate stability of $\boldsymbol{x}_{\text{eq}}$.

If nonlinearity and gravity are neglected, then Eqs. (14) and (15) can be simplified as follows for steady-state conditions:

$$\left(1 - \dot{\phi}^2_{\text{eq}} + ih_0\dot{\phi}_{\text{eq}} - in_0\right)\zeta_{\text{eq}} = h_0\exp[i(\phi_M - \pi/2)] \tag{61}$$

$$\bar{\bar{K}}_{p0}\dot{\phi}_{\text{eq}} = \bar{\bar{K}}_d + i\kappa_{\gamma 1}(\zeta_{\text{eq}} - \bar{\zeta}_{\text{eq}}) \tag{62}$$

The location of the equilibrium points for this particular case can be easily determined graphically as described in previous publications.[33–35] These equilibrium points will be used as initial iterates in determining equilibrium points of the more general cases by using the Newton–Raphson algorithm. Note that roll direction dependence of C_{l_p} and $C_{m_{\beta p}}$, which is neglected in this study, can change location and stability of equilibrium points.

Case Study

The basic finner is an unguided missile configuration that is widely used as a standard benchmark in flight dynamics. In this study the basic finner will be named basic planar finner (BPF), whereas the equivalent configuration with WAF will be named basic wrap-around finner (BWAF). Schematics of BPF and BWAF are given in Fig. 3. Reference data that are used in this case study are $D_m = 0.02$, $S_m = 3.14 \times 10^{-4}$, $a_\infty = 344$, and $\rho_\infty = 1.225$. The inertial data of the basic finner are $m = 0.15$, $I_a = 8.3 \times 10^{-6}$, $I_t = 3.5 \times 10^{-4}$, and $x_{\text{cm}} = 0.122$. These data are the same as the data of BPF models that were used by Murphy[37] in aeroballistic range tests.

C_Z and C_m data of BPF were determined by using the three-dimensional panel code of TÜBİTAK-SAGE (PANEL3D-A[38,39]) and the Missile DATCOM[40] database for $M_\infty = 3.0$, $-10 \le \alpha, \beta \le +10$ deg and $p = q = r = \dot{\alpha} = \dot{\beta} = 0$. C_Z and C_m data of BWAF were determined by using PANEL3D-A for the same conditions. Panel models of BPF and BWAF are shown in Figs. 4 and 5, respectively. Topological graphs of C_m vs α and β for BPF (Missile DATCOM), BPF (PANEL3D-A), and BWAF (PANEL3D-A) are presented in Figs. 6, 7, and 8, respectively.

C_D data of BPF was determined by using the Missile DATCOM database for $M_\infty = 3.0$, $-10 \le \alpha, \beta \le +10$ deg and $p = q = r = \dot{\alpha} = \dot{\beta} = 0$. It will be assumed that C_D data of BPF and BWAF are approximately the same. The topological graph of C_D vs α and β is presented in Fig. 9.

$C_{Z_\alpha}, a_F, C_{Z_\beta}, b_F, C^{(R)}_{Z_{\delta^2\gamma}}, C^{(I)}_{Z_{\delta^2\gamma}}, C_{m_\alpha}, a_t, C_{m_\beta}, b_t, C^{(R)}_{m_{\delta^2\gamma}}$, and $C^{(I)}_{m_{\delta^2\gamma}}$ data of both BPF and BWAF were determined by curve fitting Eqs. (4) and (5) to the corresponding C_Z and C_m data. Similarly, $C_{D_0} = 0.31$ and $a_D = 0.69$ were obtained for BPF (and BWAF) by curve fitting Eq. (8) to the C_D data. Sigma plot software was used

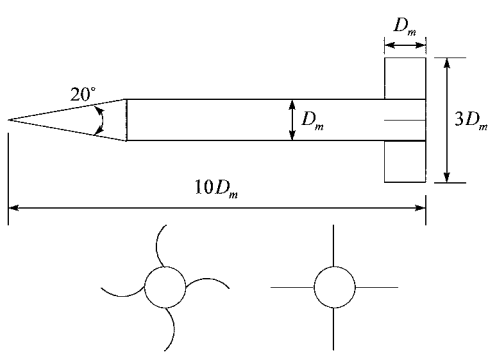

Fig. 3 BWAF and BPF configurations.

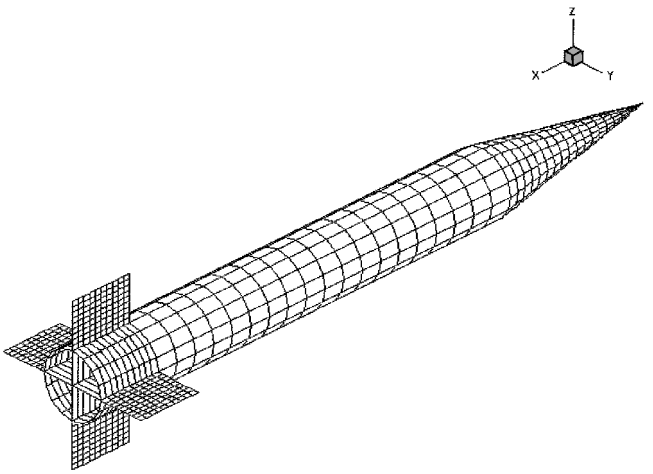

Fig. 4 Panel model of BPF.

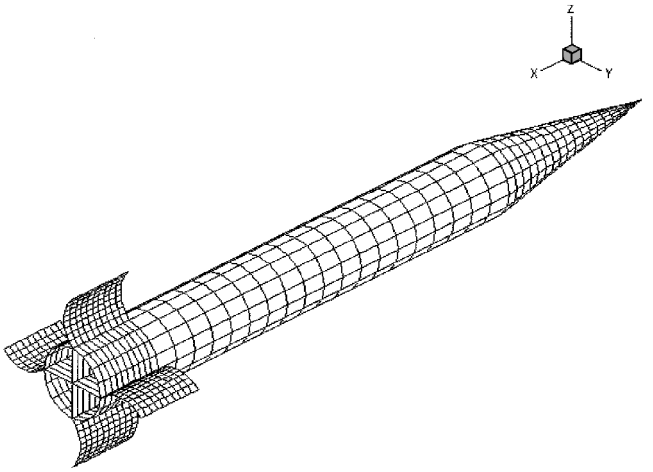

Fig. 5 Panel model of BWAF.

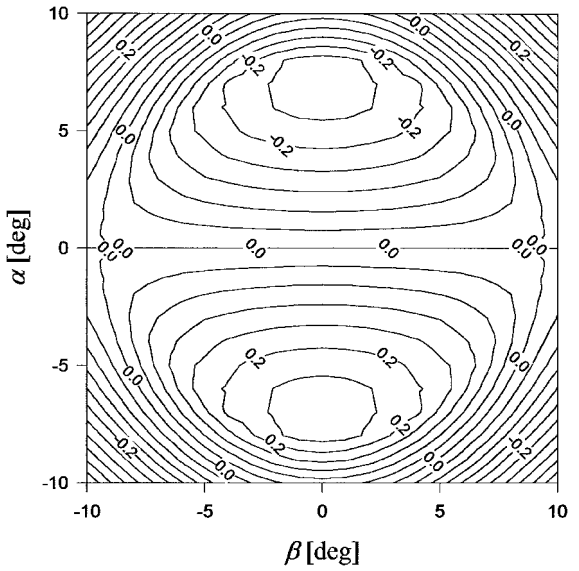

Fig. 6 BPF $C_m(\beta, \alpha)$ data for $M_\infty = 3.0$; Missile DATCOM.

in all curve fitting calculations, which all had satisfactory accuracy. Results of curve fitting are given in Tables 1 and 2 for stability derivatives and coefficients that are present in Eqs. (6–8).

The sum of damping and lag moment stability derivatives of BPF was obtained from the Missile DATCOM database as $C_{m_q} + C_{m_{\dot\alpha}} = -117.0$. The Magnus moment stability derivative of BPF for $M_\infty = 3.0$ was obtained from aeroballistic range test results of Murphy[37] as $C_{m_{\beta p}} = -8.0$. It will be assumed that $C_{m_q} + C_{m_{\dot\alpha}}$ and

Table 1 Aerodynamic force stability derivatives and coefficients for BPF and BWAF

Configuration (code)	C_{Z_α}	a_F	$C^{(R)}_{Z_{\delta^2\gamma}}$	$C^{(I)}_{Z_{\delta^2\gamma}}$
BPF (Missile DATCOM)	−8.40	6.10	0.60	0.00
BPF (PANEL3D-A)	−7.98	−1.17	−3.10	0.00
BWAF (PANEL3D-A)	−8.96	0.39	−3.15	−1.35

Table 2 Aerodynamic moment stability derivatives and coefficients for BPF and BWAF

Configuration (code)	C_{m_α}	a_t	C_{m_β}	b_t	$C^{(R)}_{m_{\delta^2\gamma}}$	$C^{(I)}_{m_{\delta^2\gamma}}$
BPF (Missile DATCOM)	−3.70	−31.40	0.00	0.00	0.00	15.50
BPF (PANEL3D-A)	−5.93	2.20	0.00	0.00	0.00	9.00
BWAF (PANEL3D-A)	−9.34	−3.49	−0.32	98.65	−5.18	9.60

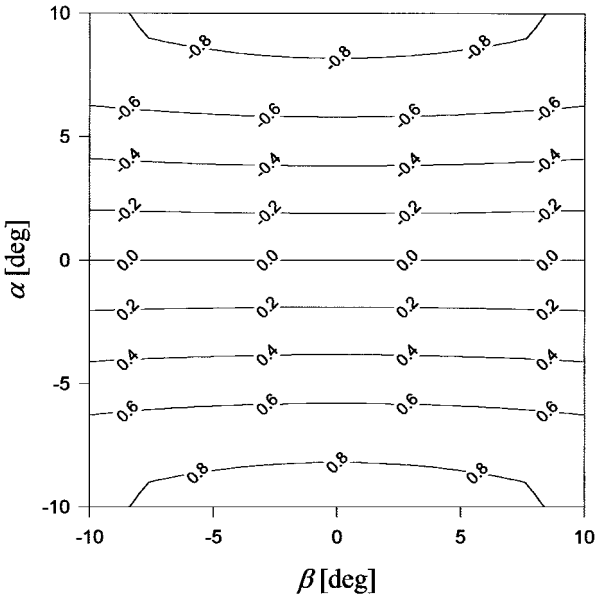

Fig. 7 BPF $C_m(\beta, \alpha)$ data for $M_\infty = 3.0$; PANEL3D-A.

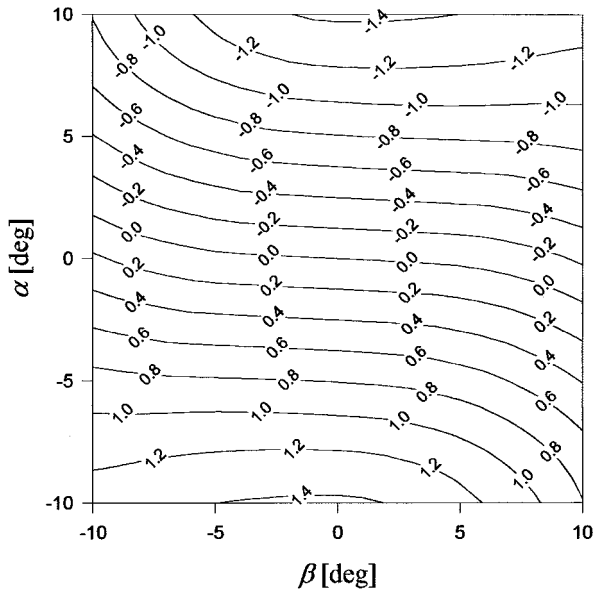

Fig. 8 BWAF $C_m(\beta, \alpha)$ data for $M_\infty = 3.0$; PANEL3D-A.

Table 3 Coefficients of axial rotational equation of motion for BPF and BWAF

Configuration	$\widehat{K}_{p_0}$	κ_{p_2}	$\widehat{\widehat{K}}_d$	κ_{γ_1}	κ_{γ_2}	κ_{γ_3}	κ_{γ_4}
A	1.5×10^{-1}	-3.3×10^{-5}	3.1×10^{-1}	1.9×10^{-1}	-7.0×10^{-3}	2.3×10^{-3}	1.4×10^{-7}
B	1.2×10^{-1}	-2.6×10^{-5}	2.4×10^{-1}	1.4×10^{-1}	1.6×10^{-3}	1.5×10^{-3}	6.4×10^{-4}

Table 4 Coefficients of transverse equation of motion for BPF and BWAF

Coefficient	Configuration A	Configuration B
$\widehat{H}_0$	8.7×10^{-2}	7.3×10^{-2}
$\widehat{H}_{2_s}$	-1.5×10^{-3}	3.7×10^{-4}
h_0	9.1×10^{-2}	7.6×10^{-2}
h_{2_s}	-1.5×10^{-3}	3.7×10^{-4}
m_{2_s}	-6.8×10^{-2}	1.1×10^{-1}
n_0	8.2×10^{-7}	-3.5×10^{-2}
n_{2_s}	5.7×10^{-6}	-1.0×10^{-1}
$s_i^{(R)}$	4.6×10^{-4}	3.7×10^{-4}
$s_i^{(I)}$	2.8×10^{-8}	1.6×10^{-4}
$r_i^{(R)}$	2.4×10^{-6}	-1.7×10^{-2}
$r_i^{(I)}$	4.6×10^{-2}	3.1×10^{-2}

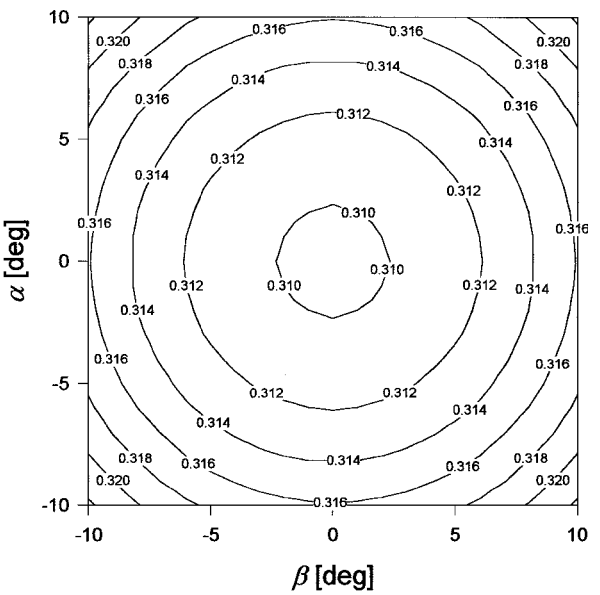

Fig. 9 BPF $C_D(\beta,\alpha)$ data for $M_\infty = 3.0$.

$C_{m_{\beta p}}$ characteristics of BPF and BWAF are approximately the same. Cubic transverse damping and cubic Magnus moments will be neglected, $d_t = 0$ and $f_t = 0$. The roll moment due to cant of tail fins coefficient and the roll damping moment stability derivative of BPF for $M_\infty = 3.0$ were obtained from the Missile DATCOM database as $C_{l_{\delta_f}} = 3.83$ and $C_{l_p} = -8.24$, respectively. $C_{l_{\delta_f}}$ and C_{l_p} data of BWAF will be assumed to be the same as that of BPF; induced roll moment will be neglected, $C_{l_0} = 0$.

Coefficients of axial rotational and transverse equations of motion for BPF and BWAF are presented in Tables 3 and 4. $C_{Z_\alpha}, a_F, C_{Z_\beta}, b_F$, $C^{(R)}_{Z_{\delta^2\gamma}}, C^{(I)}_{Z_{\delta^2\gamma}}, C_{m_\alpha}, a_t, C_{m_\beta}, b_t, C^{(R)}_{m_{\delta^2\gamma}}$, and $C^{(I)}_{m_{\delta^2\gamma}}$ data that were obtained from PANEL3D-A were used to determine these coefficients for both BPF and BWAF. $C_{m_0} = 0.095$ and 0.125 for BPF and BWAF, respectively, so that $|\delta_{T_R}| \approx 10$ deg for both cases; $\delta_f = 0.401$ and 0.659 deg for BPF and BWAF, respectively, so that design roll rate $\dot{\phi}_{ss} \approx \widehat{\widehat{K}}_d / \widehat{K}_{p_0} = 1.25$ for both cases; and $r_C = 0.04$ and $\Gamma = 0 + i0$ for both BPF and BWAF.

Figures 10 and 11 show location of equilibrium points of BPF and BWAF, respectively, for $\phi_M = 0, \ldots, 350$ deg, when all coefficients of the equations of motion except $\widehat{H}_0$, h_0, n_0, $\widehat{K}_{p_0}$, $\widehat{\widehat{K}}_d$, and κ_{γ_1} are equal to zero.

Table 5 Location and stability of equilibrium points of the first case of BPF

	Points		
Variable	1	2	3
ϕ	0.7401	0.9954	1.4667
$\zeta^{(R)}$	0.0294	0.9945	0.0091
$\zeta^{(I)}$	0.1972	0.1005	−0.0781
	Unstable	Unstable	Stable

Table 6 Location and stability of equilibrium points of the second case of BPF

	Points		
Variable	1	2	3
ϕ	0.7422	1.0698	1.4668
$\zeta^{(R)}$	0.0298	1.1489	0.0091
$\zeta^{(I)}$	0.1966	0.0800	−0.0782
	Unstable	Unstable	Stable

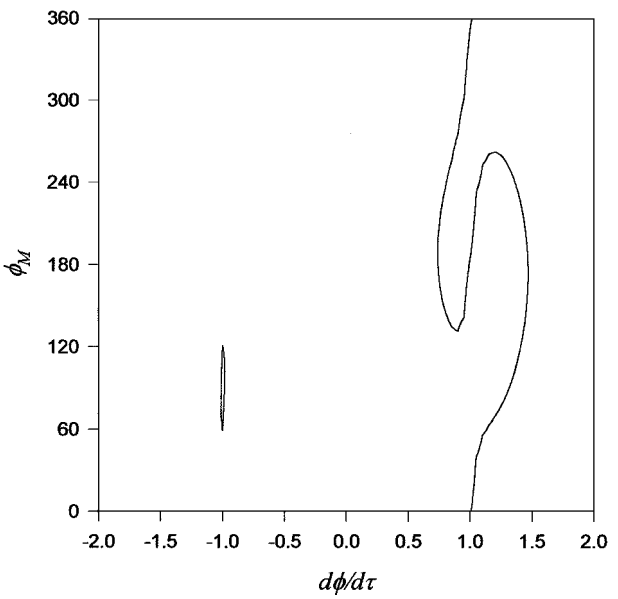

Fig. 10 Location of equilibrium points of BPF.

In Tables 5 and 6 information about location and stability of the equilibrium points of BPF is presented for two different cases ($\phi_M = 180$ deg): In the first case, coefficients of the equations of motion except $\widehat{H}_0$, h_0, $\widehat{K}_{p_0}$, $\widehat{\widehat{K}}_d$, and κ_{γ_1} were taken as zero; the location of equilibrium points was determined by using the graphical method of Murphy.[33] In the second case, coefficients of equations of motion except $\widehat{H}_0$, $\widehat{H}_{2_s}$, h_0, h_{2_s}, m_{2_s}, $s_i^{(R)}$, $r_i^{(I)}$, $\widehat{K}_{p_0}$, κ_{p_2}, $\widehat{\widehat{K}}_d$, κ_{γ_1}, κ_{γ_2}, and κ_{γ_3} were taken as zero, and the location of equilibrium points was determined iteratively by using the Newton–Raphson algorithm with an initial condition grid of 8000 equally spaced points in the $\dot{\phi} = \pm5$, $\bar{\beta} = \pm10$, and $\bar{\alpha} = \pm10$ region.

In Tables 7 and 8 information about location and stability of equilibrium points of BWAF is presented for two different cases ($\phi_M = 180$ deg): In the first case, coefficients of equations of motion except $\widehat{H}_0, h_0, n_0, \widehat{K}_{p_0}, \widehat{\widehat{K}}_d$, and κ_{γ_1} were taken as zero; the location of

Table 7 Location and stability of equilibrium points of the first case of BWAF

	Location		
Variable	1	2	3
ϕ	0.7922	0.9911	1.4188
$\zeta^{(R)}$	0.0492	0.6761	0.0105
$\zeta^{(I)}$	0.1928	0.1081	−0.0740
	Unstable	Unstable	Stable

Table 8 Location and stability of equilibrium points of the second case of BWAF

	Location		
Variable	1	2	3
ϕ	0.7917	0.9740	1.4188
$\zeta^{(R)}$	0.0526	0.5348	0.0105
$\zeta^{(I)}$	0.1929	0.1155	−0.0740
	Unstable	Unstable	Stable

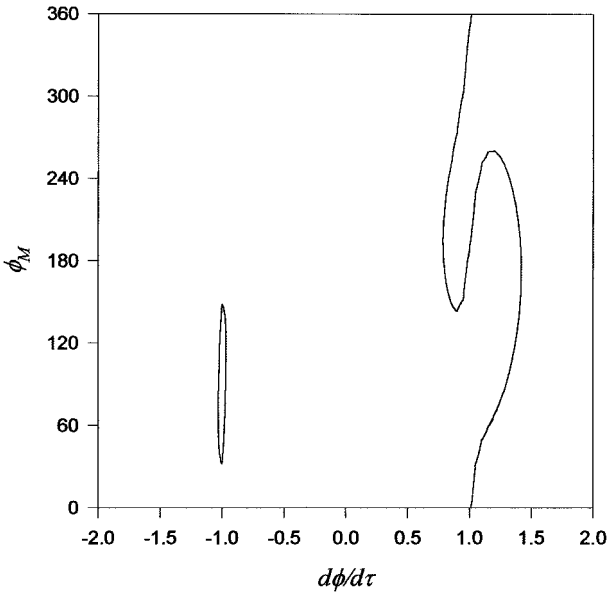

Fig. 11 Location of equilibrium points of BWAF.

equilibrium points was determined graphically. In the second case, all coefficients of the equations of motion were present, and the location of equilibrium points was determined iteratively by using the Newton–Raphson algorithm and the same initial condition grid that was used for BPF.

Note that both BPF and BWAF have three equilibrium points for the first cases as indicated by Figs. 10 and 11. There can be more equilibrium points for the second cases due to the additional nonlinear aerodynamics terms. A number of such equilibrium points were determined by using the Newton–Raphson algorithm, but in all cases the magnitude of ξ at equilibrium exceeded 10 deg. These equilibrium points will not be discussed because aerodynamic data used in this study are limited to $-10 \leq \alpha, \beta \leq +10$ deg.

A set of numerical experiments was performed in which the effects of various coefficients on the response of BWAF were investigated systematically. Equations of motion were solved by using the fourth order Runge–Kutta utility of INSITE[41] software with $\Delta\tau = 0.1$. First, all coefficients except $\bar{H}_0$, h_0, $\bar{K}_{p_0}$, $\bar{\bar{K}}_d$, n_0, and κ_{γ_1} were taken as zero, and the response was determined for $\phi_M = 270$ deg and $\boldsymbol{x}_0^T = (0, 0, 0, 0, -1)$. Five more simulations were performed with the same conditions in which more nonlinear terms were taken as nonzero successively with the following order: second simulation, κ_{p_2}, $\bar{H}_{2_s}$, and h_{2_s}; third simulation, κ_{γ_2} and m_{2_s}; fourth simulation, n_{2_s}; fifth simulation, κ_{γ_3}, $s_i^{(R)}$ and $r_i^{(I)}$; and sixth simulation, κ_{γ_4}, $s_i^{(I)}$, and $r_i^{(R)}$. Figure 12 shows variation of $\dot{\phi}$ with τ for the third simulation (stable design roll equilibrium) and the fourth simulation (unstable normal persistent resonance followed by catastrophic yaw), respectively. Results of the first and the second simulations were similar to the result of the third simulation. Results of the fifth and the sixth simulations were similar to the result of the fourth simulation.

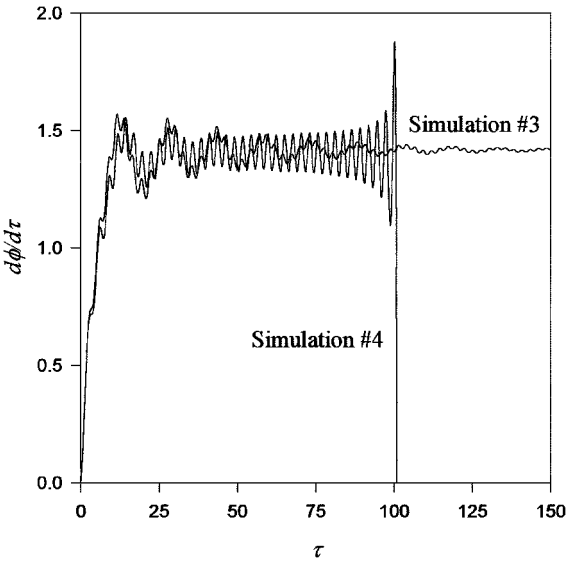

Fig. 12 Variation of $\dot{\phi}$ with τ of BWAF.

Discussion of Results

Comparison of Figs. 6 and 7 as well as examination of Tables 1 and 2 show that Missile DATCOM and PANEL3D-A predictions of transverse aerodynamics of BPF are not in good agreement for large values of ξ. Missile DATCOM predicts variation of C_Z and C_m with ξ to be much more nonlinear when compared to PANEL3D-A.

The difference between PANEL3D-A $C_m(\beta, \alpha)$ data of BPF and BWAF as indicated by Figs. 7 and 8 is significant. PANEL3D-A predicts BWAF transverse aerodynamics to be much more nonlinear when compared to that of BPF.

In previous studies, $(C_{Z_\alpha}, C_{m_\alpha})$ characteristics of configurations with WAF were reported to be almost the same as those of configurations with equivalent PF. Tables 1 and 2 show that differences between PANEL3D-A predictions for BPF and BWAF are not negligible in terms of both $(C_{Z_\alpha}, C_{m_\alpha})$ and (a_F, a_t).

In previous studies on aerodynamics and flight dynamics of WAF configurations, $|C_{m_\beta}|$ was reported to be much smaller than $|C_{m_\alpha}|$. Table 2 shows that a similar result was obtained in this study by using PANEL3D-A. On the other hand, note the large magnitude of b_t when compared to a_t in Table 2.

Tables 1 and 2 show that in case of BPF, PANEL3D-A and Missile DATCOM predictions for $C^{(I)}_{Z_{\delta^2\gamma}}$, C_{m_β}, b_t, and $C^{(R)}_{m_{\delta^2\gamma}}$ were determined to be negligible, as also indicated by Maple–Synge analysis.

Tables 1 and 2 show that PANEL3D-A predicts nonzero $C^{(I)}_{Z_{\delta^2\gamma}}$ and $C^{(R)}_{m_{\delta^2\gamma}}$ for BWAF. Also note that $|C^{(I)}_{Z_{\delta^2\gamma}}|$ and $|C^{(R)}_{m_{\delta^2\gamma}}|$ are not small when compared to $|C^{(R)}_{Z_{\delta^2\gamma}}|$ and $|C^{(I)}_{m_{\delta^2\gamma}}|$, respectively. Tables 1 and 2 show that PANEL3D-A predicts larger $|C^{(R)}_{Z_{\delta^2\gamma}}|$ and $|C^{(I)}_{m_{\delta^2\gamma}}|$ for BWAF when compared to BPF.

Table 5 shows that three equilibrium points were determined for BPF when $\phi_M = 180$ deg and all nonlinear aerodynamics terms were neglected. Only one of these equilibrium points with $\phi = 1.4667$ is stable. Table 6 shows that the location of the unstable normal persistent resonance equilibrium point with $\phi \approx 1.0$ changed significantly when nonlinear aerodynamics terms were also taken into account.

Table 7 shows that three equilibrium points were determined for BWAF when $\phi_M = 180$ deg and all nonlinear aerodynamics

terms were neglected. Only one of these equilibrium points with $\dot{\phi} = 1.4188$ is stable. Table 8 shows that the location of one of the equilibrium points (an unstable normal persistent resonance with $\dot{\phi} \approx 1.0$) changed significantly when nonlinear aerodynamics terms were also taken into account.

Figure 12 shows the significant effect of cubic out-of-plane moment characterized by the coefficient b_t on the nature of response. In case of unguided missiles with PF, induced transverse moment that is characterized by the coefficient $C_{m_{\delta^2\gamma}}$ is the source of catastrophic yaw behavior. On the other hand, cubic out-of-plane moment was determined to be the source of catastrophic yaw behavior in the case of BWAF.

Conclusions

Research on aerodynamics of missile configurations with WAF has focused mainly on investigation of linear out-of-plane moment C_{m_β}, induced roll moment C_{l_0}, and roll direction dependence of roll damping stability derivative $C_{l_{p\pm}}$. Flight dynamicists have performed linear stability analysis of WAF configurations by considering C_{m_β} to be the only out-of-plane effect due to lack of mirror symmetry. Nonlinear transverse aerodynamics, nonlinear yaw–pitch motions, and nonlinear coupled yaw–pitch–roll motions of unguided missiles with WAF have remained as untouched problems until now.

In this study, a general nonlinear aerodynamics model and nonlinear coupled axial and transverse equations of motion for unguided missiles with four WAF are presented for the first time. The equations of motion can be used for a wide variety of analysis, synthesis, and identification work. It is shown that the difference between transverse aerodynamics of unguided missiles with WAF and PF is not minor especially at relatively large values of magnitude of total angle of attack. Hence, it is not possible to perform accurate flight dynamics analysis of a WAF configuration by treating it as a minor linear deviation from its equivalent with PF. Cubic static out-of-plane moment, which was never considered in modeling of unguided missiles with WAF before, was determined to have significant effects on response characteristics.

Aerodynamic data used in this study were obtained from the Missile DATCOM empirical database, three-dimensional panel code PANEL3D-A, and available results of aeroballistic range tests. Because Missile DATCOM does not have any capability for configurations with WAF, nonlinear transverse WAF aerodynamic data had to be determined by using PANEL3D-A. On the other hand, the accuracy of PANEL3D-A WAF data is questionable because PANEL3D-A and Missile DATCOM predictions for a planar finned configuration were shown to be significantly different in the case study section. Research on determination of WAF aerodynamics data from aeroballistic range test results is in progress. Research on determination of WAF aerodynamics data by using advanced computational fluid dynamics is in progress. Further research is recommended to be carried out on roll direction dependence of WAF aerodynamics, on variation of WAF drag force with total angle of attack, and on periodic, quasi-periodic and aperiodic behavior of missile configurations with WAF. Further research is recommended to be carried out on nonlinear flight dynamics of missile configurations with three WAF (such as 2.75-in. Mk 66) because Maple–Synge analysis shows that nonlinearity increases when the number of fins decreases.

References

[1]Dahlke, C. W., and Craft, J. C., "The Effect of Wrap-Around Fins on Aerodynamic Stability and Rolling Moment Variations," U.S. Army Missile Research Development and Engineering Lab., RD-73-17, Redstone Arsenal, AL, July 1973.

[2]Stevens, F. L., "Analysis of the Linear Pitching and Yawing Motion of Curved Finned Missiles," Naval Weapons Lab., NWL TR-2989, Dahlgren, VA, Oct. 1973.

[3]Stevens, F. L., On, T. J., and Clare, T. A., "Wrap-Around vs Cruciform Fins: Effects on Rocket Flight Performance," AIAA Paper 74-777, Aug. 1974.

[4]Daniels, P., and Hardy, S. R., "Roll Rate Stabilization of a Missile Configuration with Wrap-Around Fins," *Journal of Spacecraft and Rockets*, Vol. 13, No. 7, 1975, pp. 446–448.

[5]Whyte, R. H., Hathaway, W. H., Buff, R. S., and Winchenbach, G. L., "Subsonic and Transonic Aerodynamics of a Wrap-Around Fin Configuration," AIAA Paper 85-0106, Jan. 1985.

[6]Kim Hoon, Y., and Winchenbach, G. L., "Roll Motion of a Wrap-Around Fin Configuration at Subsonic and Transonic Mach Numbers," *Journal of Guidance, Control, and Dynamics*, Vol. 9, No. 2, 1986, pp. 253–255.

[7]Winchenbach, G. L., Buff, R. S., Whyte, R. H., and Hathaway, W. H., "Subsonic and Transonic Aerodynamics of a Wrap-Around Fin Configuration," *Journal of Guidance, Control, and Dynamics*, Vol. 9, No. 6, 1986, pp. 627–632.

[8]Vitale, R. E., Abate, G. L., Winchenbach, G. L., and Riner, W., "Aerodynamic Test and Analysis of a Missile Configuration with Curved Fins," AIAA Paper 92-4495, 1992.

[9]Tanrıkulu, Ö., Önen, C., Mahmutyazıcıoğlu, G., and Bektaş, İ., "Linear Stability Analysis of Unguided Missiles with Wrap-Around Tail Fins in Free Flight," AGARD Flight Vehicle Integration Panel Specialist Meeting on Subsystem Integration for Tactical Missiles, Paper 5, Oct. 1995.

[10]Abate, G. L., and Winchenbach, G. L., "Analysis of Wrap-Around Fin and Alternate Deployable Fin Systems for Missiles," AGARD Flight Vehicle Integration Panel Specialist Meeting on Subsystem Integration for Tactical Missiles, Paper 4, Oct. 1995.

[11]Tanrıkulu, Ö., and Mahmutyazıcıoğlu, G., "Magnus Effects on Stability of Wrap-Around Finned Missiles," *Journal of Spacecraft and Rockets*, Vol. 35, No. 4, 1998, pp. 467–472.

[12]Hardy, S. R., "Non-Linear Analysis of the Rolling Motion of a Wrap-Around Fin Missile at Angles of Attack from 0° to 90° in Compressible Flow," U.S. Naval Surface Weapons Center, NSWC/DL-TR-3727, Dahlgren, VA, Sept. 1977.

[13]Asrar, W., Baig, M. F., and Khan, S. A., "Chaos in WAF Projectile Motion," AIAA Paper 96-0066, Jan. 1996.

[14]Nicolaides, J. D., "On the Free Flight Motion of Missiles Having Slight Configurational Asymmetries," U.S. Army Ballistic Research Lab., BRL Rept. 858, AD 26405, Aberdeen Proving Ground, MD, 1952.

[15]Glover, L. S., "Effects on Roll Rate of Mass and Aerodynamic Asymmetries for Ballistic Re-Entry Bodies," *Journal of Spacecraft and Rockets*, Vol. 2, No. 2, 1965, pp. 220–225.

[16]Nicolaides, J. D., "A Review of Some Recent Progress in Understanding Catastrophic Yaw," Rept. 551, AGARD, 1966.

[17]Daniels, P., "Fin-Slots Versus Roll Lock-In and Roll Speed Up," *Journal of Spacecraft and Rockets*, Vol. 4, No. 3, 1967, pp. 410–412.

[18]Chadwick, W. R., "Flight Dynamics of a Bomb with Cruciform Tail," *Journal of Spacecraft and Rockets*, Vol. 4, No. 6, 1967, pp. 768–773.

[19]Platus, D. H., "Note on Re-Entry Vehicle Roll Resonance," *AIAA Journal*, Vol. 5, No. 7, 1967, pp. 1348–1350.

[20]Price, D. A., Jr., "Sources, Mechanisms, and Control of Roll Resonance Phenomena for Sounding Rockets," *Journal of Spacecraft and Rockets*, Vol. 4, No. 11, 1967, pp. 1516–1525.

[21]Vaughn, H. R., "Boundary Conditions for Persistent Roll Resonance on Re-Entry Vehicles," *AIAA Journal*, Vol. 6, No. 6, 1968, pp. 1030–1035.

[22]Barbera, F. J., "An Analytical Technique for Studying the Anomalous Roll Behavior of Re-Entry Vehicles," *Journal of Spacecraft and Rockets*, Vol. 6, No. 11, 1969, pp. 1279–1284.

[23]Nayfeh, A. H., "A Multiple Time Scaling Analysis of Re-Entry Roll Dynamics," *AIAA Journal*, Vol. 7, No. 11, 1969, pp. 2155–2157.

[24]Daniels, P., "A Study of the Non-Linear Rolling Motion of a Four-Finned Missile," *Journal of Spacecraft and Rockets*, Vol. 7, No. 4, 1970, pp. 510–512.

[25]Price, D. A., Jr., and Ericsson, L. E., "A New Treatment for Roll-Pitch Coupling for Ballistic Re-Entry Vehicles," *AIAA Journal*, Vol. 8, No. 9, 1970, pp. 1608–1615.

[26]Clare, T. A., "Resonance Instability for Finned Configurations Having Non-Linear Aerodynamic Properties," *Journal of Spacecraft and Rockets*, Vol. 8, No. 3, 1971, pp. 278–283.

[27]Bootle, W. J., "Spin Variations in Slender Entry Vehicles During Rolling Trim," *AIAA Journal*, Vol. 9, No. 4, 1971, pp. 729–731.

[28]Madden, R. G., "Statistical Analysis of the Roll Rate of a Launch Vehicle Under the Influence of Random Fin Misalignments," *AIAA Journal*, Vol. 10, No. 3, 1972, pp. 324, 325.

[29]Nayfeh, A. H., and Saric, W. S., "Analysis of Asymmetric Rolling Bodies with Nonlinear Aerodynamics," *AIAA Journal*, Vol. 10, No. 8, 1972, pp. 1004–1011.

[30]Cohen, C. J., Clare, T., and Stevens, F. L., "Analysis of the Nonlinear Rolling Motion of Finned Missiles," *AIAA Journal*, Vol. 12, No. 3, 1974, pp. 303–309.

[31]Pepitone, T. R., and Jacobson, I. D., "Resonant Behavior of a Symmetric Missile Having Roll Orientation-Dependent Aerodynamics," *Journal of Guidance, Control, and Dynamics*, Vol. 1, No. 5, 1978, pp. 335–339.

[32]Bennett, M. D., "Roll Resonance Probability for Ballistic Missiles with Random Configurational Asymmetry," *Journal of Guidance, Control, and Dynamics*, Vol. 6, No. 3, 1983, pp. 222–224.

[33]Murphy, C. H., "Some Special Cases of Spin-Yaw Lock-In," *Journal of*

Guidance, Control, and Dynamics, Vol. 12, No. 6, 1989, pp. 771–776.

[34]Ananthkrishnan, N., and Raisinghani, S. C., "Steady and Quasisteady Resonant Lock-In of Finned Projectiles," *Journal of Spacecraft and Rockets*, Vol. 29, No. 5, 1992, pp. 692–696.

[35]Tanrıkulu, Ö., "Limit Cycle and Chaotic Behavior in Persistent Resonance of Unguided Missiles," *Journal of Spacecraft and Rockets*, Vol. 36, No. 6, 1999, pp. 859–865.

[36]Nielsen, J. N., *Missile Aerodynamics*, Nielsen Engineering and Research, Inc., Mountain View, CA, 1988, pp. 358–363.

[37]Murphy, C. H., "Free Flight Motion of Symmetric Missiles," Ballistic Research Lab., Rept. 1216, Aberdeen Proving Ground, MD, July 1963.

[38]Gökhan, T., and Önen, C., "Panel Project Final Report," TÜBİTAK-SAGE, Rept. SAGE-A5-RA-MS-0003, Ankara, Turkey, Feb. 1998.

[39]Önen, C., "Aerodynamic Analysis of Complex Missile Geometries by Panel Methods," M.S. Thesis, Dept. of Aeronautical Engineering, Middle East Technical Univ., Ankara, Turkey, June 1996.

[40]Blake, W. B., "Missile DATCOM: 1997 Status and Future Plans," AIAA Paper 97-2280, June 1997.

[41]Parker, T. S., and Chua, L. O., *Practical Numerical Algorithms for Chaotic Systems*, Springer-Verlag, New York, 1989, pp. 237–269.

M. S. Miller
Associate Editor